$S=-1$ meson-baryon unitarized coupled channel chiral perturbation theory and the S_{01} resonances $\Lambda(1405)$ and $-\Lambda(1670)$

C. García-Recio,* J. Nieves,† and E. Ruiz Arriola‡
Departamento de Física Moderna, Universidad de Granada, E-18071 Granada, Spain

M. J. Vicente Vacas
Departamento Fisica Teórica and IFIC, Centro mixto Universidad de Valencia–CSIC, Aptd. 22085, E-46071 Valencia, Spain
(Received 18 October 2002; published 29 April 2003)

The s-wave meson-baryon scattering is analyzed for the strangeness $S=-1$ and isospin $I=0$ sector in a Bethe-Salpeter coupled channel formalism incorporating chiral symmetry. Four channels have been considered: $\pi\Sigma$, $\bar{K}N$, $\eta\Lambda$, and $K\Xi$. The required input to solve the Bethe-Salpeter equation is taken from lowest order chiral perturbation theory in a relativistic formalism. There appear undetermined low energy constants, as a consequence of the renormalization of the amplitudes, which are obtained from fits to the $\pi\Sigma\to\pi\Sigma$ mass spectrum, to the elastic $\bar{K}N\to\bar{K}N$ and $\bar{K}N\to\pi\Sigma$ t matrices and to the $K^-p\to\eta\Lambda$ cross section data. The position and residues of the complex poles in the second Riemann sheet of the scattering amplitude determine the masses, widths, and branching ratios of the S_{01} resonances $\Lambda(1405)$ and $-\Lambda(1670)$, in reasonable agreement with experiment. A good overall description of the data, from the $\pi\Sigma$ threshold up to 1.75 GeV, is achieved despite the fact that three-body channels have not been explicitly included.

DOI: 10.1103/PhysRevD.67.076009 PACS number(s): 11.10.St, 11.30.Rd, 11.80.Et

I. INTRODUCTION

Baryon resonances are outstanding features in elastic and inelastic meson-baryon scattering and signal the onset of nonperturbative physics. Constituent quark model approaches describe them as excited baryonic bound states, and the coupling to the continuum is obtained by evaluating transition matrix elements [1], but comparison with data can be done only once the scattering problem is solved. In such a scheme, the underlying quark constituent nature of hadrons is taken into account but implementation of chiral symmetry (CS) becomes difficult. In the region of low energies, it seems appropriate to start considering the hadrons as the relevant degrees of freedom, where CS not only proves helpful to restrict the type of interactions between mesons and baryons, but also provides an indirect link to the underlying quantum chromodynamics (QCD) [2]. For processes involving baryons and mesons, heavy baryon chiral perturbation theory (HBChPT) [3,4] incorporates CS at low energies in a systematic way, and has provided a satisfactory description of πN scattering in the region around threshold [5–7]. It suffers, however, from known limitations. First, the expansion is manifestly not relativistically invariant, and some convergence problems, especially for the scalar form factor, have been pointed out and solved by defining a suitable regularization scheme, the so-called infrared regularization (IR) [8]. The IR scheme has also successfully been applied to πN elastic scattering [9]. The previous remarks concern a theory with only π and N present. The Δ degrees of freedom have been explicitly included [10] within the HBChPT scheme, where the nucleon-Δ splitting is considered to be of the order of the pion mass, pointing toward a better convergence for the πN scattering data than in the case without explicit Δ's. More recently, the work of Ref. [11] has compared the HBChPT scheme to the IR one in the presence of explicit Δ degrees of freedom for πN scattering, showing that HBChPT describes data up to much higher pion c.m. kinetic energies than the IR method.

A second limitation of any of the previous approaches, both in the HBChPT as well as in the IR frameworks and with or without explicit Δ, is that they are based on a perturbative expansion of a finite number of Feynman diagrams. This complies with unitarity order by order in the expansion, but fails to satisfy exact unitarity of the scattering amplitude. Thus, some nonperturbative resummation should be supplemented to incorporate exact unitarity and, hopefully, to accommodate resonances. Regarding this second limitation, several unitarization methods have been suggested in the literature and previously used to describe the meson-baryon dynamics: inverse amplitude method (IAM) [12], or a somewhat modified IAM to account for the large baryon masses [13], dispersion relations [14–16], the Lippmann-Schwinger equation (LSE), and the Bethe-Salpeter equation (BSE) [17–26].

In this work, we will study the s-wave meson-baryon scattering for the strangeness $S=-1$ and isospin $I=0$ sector in a Bethe-Salpeter coupled channel formalism incorporating CS. This reaction provides a good example of the need for unitarization methods; the recent work of Ref. [27] shows that HBChPT to one loop already fails completely at threshold. The $\bar{K}N$ scattering length turns out to have a real part about the same size but with opposite sign and half the imaginary part expected experimentally [28], due to the nearby subthreshold $\Lambda(1405)$ resonance. It is important to realize from the very beginning that, for this particular reso-

*Email address: g_recio@ugr.es
†Email address: jmnieves@ugr.es
‡Email address: earriola@ugr.es

nance, the unitarization program implies considering at least two channels, namely, $\pi\Sigma$ and $\bar{K}N$. Thus, one deals with a coupled channel problem. Unfortunately, there are no one-loop ChPT calculations incorporating this coupled channel physics. Much of the discussion below and in the rest of the paper reflects this lack of knowledge on the general structure of this scattering amplitude within ChPT, particularly on the number of undetermined parameters. Of course, not all counterterms are independent, as demanded by crossing and chiral symmetries. Actually, the best practical way to impose these constraints on a unitarized partial wave amplitude is by matching to a ChPT amplitude. The reason for this is that the left-cut partial wave analytical structure implied by crossing would be automatically incorporated within a one-loop ChPT calculation. This point of view has been used in several unitarization approaches for the elastic πN process [15,12–14]. There, the ChPT amplitude is known up to one loop [5–7,9], which in HBChPT corresponds to third and fourth order. This is the lowest order approximation incorporating the perturbative unitarity correction which is required to match the perturbative amplitude to a unitarized one. As we have already mentioned, the coupled channel ChPT one-loop amplitude for meson-baryon scattering is not known, and thus the matching is not possible.

The first study of the strangeness $S=-1$ and isospin $I=0$ meson-baryon channel incorporating CS and coupled channel unitarization was carried out in Refs. [18,19], although some phenomenological form factors were employed. More recently, this channel has been studied in Refs. [21] and [22], where a three-momentum cutoff is used to renormalize the LSE and the off-shell behavior is partially taken into account. In principle, the minimal renormalization procedure used in Refs. [21,22] is acceptable but may turn out to be too restrictive in practice. If, instead, one takes advantage of the flexibility allowed by the renormalization of an effective field theory (EFT), there is a chance of improving the description from threshold up to higher energies. In practical terms this means increasing the number of counterterms that one has to add to make finite the amplitudes. Along the lines of Ref. [25], we will adopt this viewpoint below by taking fully into account the off-shellness suggested by the BSE using the tree level amplitude as the lowest order approximation to the potential. In the approach of Ref. [25] there are three parameters for each channel. In the absence of a one-loop ChPT coupled channel amplitude, we content ourselves with matching to the tree level one.[1] One could also match the coupled channel unitarized amplitude to HBChPT, much below the inelastic thresholds. This procedure was investigated in Ref. [25] for the πN system, but did not introduced any powerful constraints.

Despite the great success of the model of Ref. [21] in describing the data around the antikaon-nucleon threshold, including the features of the S_{01} $\Lambda(1405)$ resonance, its predictions for higher energies [22] do not work so well and clear discrepancies with data appear. Indeed, the limitations of the model of Ref. [21] already appeared in the strangeness $S=0$ and isospin $I=1/2$ meson-baryon sector, where the model is able to describe data only in a more or less narrow energy window around the $N(1535)$ resonance [23,24]. However, the model previously developed by two of us for the latter channel in Ref. [25] describes data in a wider energy region, ranging from the πN threshold up to almost a center of mass (c.m.) meson-baryon energy of $\sqrt{s}=2$ GeV, including the features of a second resonance $[N(1650)]$. Motivated by these encouraging results we extend in this work the model of Ref. [25] to the strangeness $S=-1$ and isospin $I=0$ meson-baryon channel. As in the $S=0$ sector, taking into account the off-shellness of the BSE generates a rich structure of unknown constants which allow for a better description of the amplitudes. Although the generation of more undetermined constants may appear a less predictive approach than using a cutoff (one single parameter) to regularize the divergent integrals, it reflects the real state of the art of our lack of knowledge on the underlying QCD dynamics. The number of adjustable low energy constants (LEC's) should not be smaller than those allowed by the symmetry; this is the only way both to falsify all possible theories embodying the same symmetry principles and to widen the energy interval that is being described. Limiting such a rich structure allowed by CS results in a poor description of experimental data. However, a possible redundancy of parameters is obviously undesirable but may be detected through statistical considerations (see below). The number of LEC's is controlled to any order of the calculation by crossing symmetry. In a unitarized approach, the only way to avoid this parameter redundancy is to match the unitarized amplitude to the one obtained from a Lagrangian formalism.[2] There is no standard one-loop ChPT calculation for the meson-baryon reaction with open channels to compare with. Some results exist within the HBChPT scheme, up to order $\mathcal{O}(1/(M^3 f_\pi^2),1/(M f_\pi^4))$—$M$ being a typical baryon mass—but only involving pions and nucleons [7]. An indirect way to detect such a parameter redundancy might be through a fit to experimental data if the errors and correlations in some parameters turn out to be very large. We will adopt this point of view in this work, and will show that indeed correlations take place, effectively reducing the total number of independent parameters.

In this paper four coupled channels have been considered: $\pi\Sigma$, $\bar{K}N$, $\eta\Lambda$, and $K\Xi$, and we have taken into account SU(3) symmetry breaking effects but neglected the considerably smaller isospin violation effects. We also neglected three-body channels, mainly for technical reasons. According to Ref. [33] the $\Lambda(1670)$ resonance decays into a $\Sigma^*\pi N$ three-body final state with a small (0.08 ∓ 0.06) branching ratio.

[1]This point was discussed at length in Ref. [29] in the context of elastic $\pi\pi$ scattering; from there one easily realizes that the renormalization scheme pursued in Ref. [21] would lead to a scenario where only one of the four SU(2) Gasser-Leutwyler $\bar{l}_1$, $\bar{l}_2$, $\bar{l}_3$, and $\bar{l}_4$ parameters is independent.

[2]See the discussion in Appendix D of Ref. [25].

Preliminary results of the present work can be found in [30–32].

The paper is organized as follows. In Sec. II, a summary of the theoretical framework used is described. Further details can be found in Ref. [25]. Numerical results for the amplitudes and cross sections and details of the fitting procedure are given in Sec. III. Special attention is paid both to the analytical properties, in the complex plane, of the t matrix found and to the statistical correlations between the fitted LEC's. Appendixes A and B are devoted to these issues as well. Finally, in Sec. IV we outline the conclusions of our work.

II. THEORETICAL FRAMEWORK

The coupled channel scattering amplitude for the baryon-meson process in the isospin channel $I=0$,

$$B(M_A,P-k,s_A)+M(m_A,k) \rightarrow B(M_B,P-k',s_B)+M(m_B,k'), \tag{1}$$

with baryon (meson) masses M_A and M_B (m_A and m_B) and spin indices (helicity, covariant spin, etc.) s_A, s_B, is given by

$$T_P[B\{k',s_B\}\leftarrow A\{k,s_A\}] = \overline{u}_B(P-k',s_B)t_P(k,k')u_A(P-k,s_A). \tag{2}$$

Here, $u_A(P-k,s_A)$ and $u_B(P-k',s_B)$ are baryon Dirac spinors[3] for the ingoing and outgoing baryons, respectively, P is the conserved total four-momentum, and $t_P(k,k')$ is a matrix in the Dirac and coupled channel spaces. On the mass shell the parity and Lorentz invariant amplitude t_P can be written as

$$t_P(k,k')|_{\text{on shell}}=t_1(s,t)\not{P}+t_2(s,t) \tag{3}$$

with $s=P^2=\not{P}^2$, $t=(k-k')^2$, and t_1 and t_2 matrices in the coupled channel space.

In terms of the matrices t_1 and t_2 defined in Eq. (3), the s-wave coupled channel matrix $f_0^{1/2}(s)$ $[f_L^J]$ is given by

$$[f_0^{1/2}(s)]_{B\leftarrow A}=-\frac{1}{8\pi\sqrt{s}}\sqrt{|\vec{k}_B|/|\vec{k}_A|}\sqrt{E_B+M_B}\sqrt{E_A+M_A} \times\left[\frac{1}{2}\int_{-1}^{1}d(\cos\theta)\,[\sqrt{s}t_1(s,t)+t_2(s,t)]_{BA}\right] \tag{4}$$

where the c.m. three-momentum moduli read

$$|\vec{k}_i|=\frac{\lambda^{1/2}(s,M_i^2,m_i^2)}{2\sqrt{s}},\quad i=A,B, \tag{5}$$

with $\lambda(x,y,z)=x^2+y^2+z^2-2xy-2xz-2yz$ and $E_{A,B}$ the baryon c.m. energies. The phase of the matrix T_P is such that the relation between the diagonal elements ($A=B$) in the coupled channel space of $f_0^{1/2}(s)$ and the inelasticities (η) and phase shifts (δ) is the usual one:

$$[f_0^{1/2}(s)]_{AA}=\frac{1}{2i|\vec{k}_A|}[\eta_A(s)e^{2i\delta_A(s)}-1]. \tag{6}$$

Further details of normalizations and definitions of the amplitudes can be seen in Sec. II B of Ref. [25].

To compute the amplitude t_P we solve the BSE [see Fig. 1]

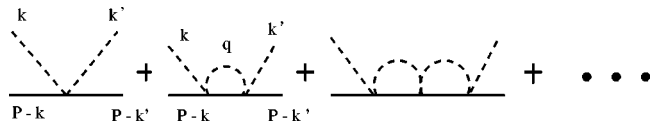

FIG. 1. Diagrams summed by the Bethe Salpeter equation. Kinematics defined in the main text.

$$t_P(k,k')=v_P(k,k')+i\int\frac{d^4q}{(2\pi)^4}t_P(q,k') \times\Delta(q)S(P-q)v_P(k,q), \tag{7}$$

where $t_P(k,k')$ is the scattering amplitude defined in Eq. (2), $v_P(k,k')$ is the two-particle irreducible Green's function (or potential), and $S(P-q)$ and $\Delta(q)$ are the baryon and meson exact propagators, respectively. The above equation turns out to be a matrix one, in both the coupled channel and Dirac spaces. For any choice of the potential $v_P(k,k')$, the resulting scattering amplitude $t_P(k,k')$ satisfies the coupled channel unitarity condition, discussed in Eq. (21) of Ref. [25]. The BSE requires some input potential and baryon and meson propagators to be solved. To compute the lowest order of the BSE-based expansion [29] it is enough to approximate the iterated potential by the chiral expansion lowest order meson-baryon amplitudes in the desired strangeness and isospin channel, and the intermediate particle propagators by the free ones (which are diagonal in the coupled channel space). From the meson-baryon chiral Lagrangian [2] (see Sec. II A of Ref. [25]), one gets at lowest order for the potential

$$v_P(k,k')=t_P^{(1)}(k,k')=\frac{D}{f^2}(\not{k}+\not{k}') \tag{8}$$

with D the coupled channel matrix

$$D_{S=-1}^{I=0}=\frac{1}{4}\begin{array}{c} \begin{matrix} \overline{K}N & \pi\Sigma & \eta\Lambda & K\Xi \end{matrix} \\ \begin{pmatrix} -3 & \sqrt{3/2} & -3/\sqrt{2} & 0 \\ \sqrt{3/2} & -4 & 0 & -\sqrt{3/2} \\ -3/\sqrt{2} & 0 & 0 & 3/\sqrt{2} \\ 0 & -\sqrt{3/2} & +3/\sqrt{2} & -3 \end{pmatrix} \end{array} \begin{matrix} \overline{K}N \\ \pi\Sigma \\ \eta\Lambda \\ K\Xi \end{matrix} \tag{9}$$

given in the isospin basis and the same phase conventions as in Ref. [25].

While amplitudes follow the chiral symmetry breaking pattern from the effective Lagrangian to a good approxima-

[3]We use the normalization $\overline{u}u=2M$.

tion, it is well known that physical mass splittings have an important influence when calculating the reaction phase space. Indeed, the correct location of reaction thresholds requires taking physical masses for the corresponding reaction channels. We have taken this effect into account in our numerical calculation. We also incorporate explicit CS effects in the weak meson decay constants and different numerical values for f_π, f_K, and f_η can be used. This can be easily accomplished through the prescription

$$D/f^2 \to \hat{f}^{-1} D \hat{f}^{-1}, \quad \hat{f} = \mathrm{diag}(f_K, f_\pi, f_\eta, f_K). \tag{10}$$

The solution of the BSE with the kernel specified above can be found in Ref. [25]. It turns out that the functions t_1 and t_2, defined in Eq. (3), do not depend on the Mandelstam variable t, and thus the dynamics is governed by the matrix function $t(s)$ [see Eq. (4)]

$$t(s) = \sqrt{s}\, t_1(s) + t_2(s), \tag{11}$$

which is given in Eq. (34) of Ref. [25]. There, the renormalization of the amplitudes obtained is studied at length. As a result of the renormalization procedure, and in addition to the physical masses and weak meson decay constants, a total number of 12,

$$\begin{array}{cccc} J_{\bar{K}N}, & J_{\pi\Sigma}, & J_{\eta\Lambda}, & J_{K\Xi}, \\ \Delta_N, & \Delta_\Sigma, & \Delta_\Lambda, & \Delta_\Xi, \\ \Delta_{\bar{K}}, & \Delta_\pi, & \Delta_\eta, & \Delta_K, \end{array} \tag{12}$$

undetermined LEC's appear. We fit these constants to data, as we will see in the next section, and from them we define the three following diagonal matrices:

$$J_0(s=(\hat{m}+\hat{M})^2) = \begin{pmatrix} J_{\bar{K}N} & 0 & 0 & 0 \\ 0 & J_{\pi\Sigma} & 0 & 0 \\ 0 & 0 & J_{\eta\Lambda} & 0 \\ 0 & 0 & 0 & J_{K\Xi} \end{pmatrix},$$

$$\Delta_{\hat{M}} = \begin{pmatrix} \Delta_N & 0 & 0 & 0 \\ 0 & \Delta_\Sigma & 0 & 0 \\ 0 & 0 & \Delta_\Lambda & 0 \\ 0 & 0 & 0 & \Delta_\Xi \end{pmatrix},$$

$$\Delta_{\hat{m}} = \begin{pmatrix} \Delta_{\bar{K}} & 0 & 0 & 0 \\ 0 & \Delta_\pi & 0 & 0 \\ 0 & 0 & \Delta_\eta & 0 \\ 0 & 0 & 0 & \Delta_K \end{pmatrix}, \tag{13}$$

which appear in the solution of the BSE. We have denoted the meson-baryon low energy constants $J_0(s=(m_i+M_j)^2)$, $i=\bar{K}, \pi, \eta, K$ and $j=N, \Sigma, \Lambda, \Xi$, of Eq. (A8) of Ref. [25] as J_{ij}.

III. NUMERICAL RESULTS

Throughout the paper we will use the following numerical values for the masses and weak decay constants of the pseudoscalar mesons (all in MeV):

$$\begin{aligned} & m_K = m_{\bar{K}} = 493.68, \quad m_\pi = 139.57, \quad m_\eta = 547.3, \\ & M_p = 938.27, \quad M_\Sigma = 1189.37, \quad M_\Lambda = 1115.68, \\ & M_\Xi = 1318.0, \\ & f_\pi = f_\eta = f_K = 1.15 \times 93.0, \end{aligned} \tag{14}$$

where for the weak meson decay constants we take for all channels an averaged value.[4] This selection of the coupling constants does not omit the essential features of the meson-baryon system since a recent work [34] shows that the observed SU(3) breaking in meson-baryon scatterings cannot be explained by the present SU(3) breaking interactions and that the essential physics of the resonances seems to lie in the substraction constants.

A. Fitting procedure

We perform a χ^2 fit, with 12 free parameters, to the following set of experimental data and conditions.

$S_{01}(S_{2T2J})$ $\bar{K}N \to \bar{K}N$ and $\bar{K}N \to \pi\Sigma$ scattering amplitudes (real and imaginary parts) [35], in the c.m. energy range of $1480 \leqslant \sqrt{s} \leqslant 1750$ MeV. In this c.m. energy region, there are a total number of 56 data points (28 real and 28 imaginary parts) for each channel. The normalization used in Ref. [35] is different from that used here and their amplitudes T_{ij}^{Go77} are related to ours by

$$T_{ij}^{\mathrm{Go77}} = \mathrm{sgn}(i,j) |\vec{k}_i| [f_0^{1/2}(s)]_{j \leftarrow i}, \tag{15}$$

where sgn(i,j) is $+1$ for the elastic channel and -1 for the $\bar{K}N \to \pi\Sigma$ one. On the other hand, and because in Ref. [35] errors are not provided, we have taken for those amplitudes errors given by

$$\delta T_{ij}^{\mathrm{Go77}} = \sqrt{(0.12 T_{ij}^{\mathrm{Go77}})^2 + 0.05^2} \tag{16}$$

in the spirit of those used in Ref. [36].

$S_{01} - \pi\Sigma$ mass spectrum [37], $1330 \leqslant \sqrt{s} \leqslant 1440$ MeV. In this c.m. energy region, there are a total of thirteen 10 MeV bins and the experimental data are given in arbitrary units. To compare with data, taking into account the experimental acceptance of 10 MeV, we compute

$$\frac{\Delta\sigma}{\Delta[M_{\pi\Sigma}(i)]} = C \int_{M_{\pi\Sigma}(i)-5\ \mathrm{MeV}}^{M_{\pi\Sigma}(i)+5\ \mathrm{MeV}} |[f_0^{1/2}(s=x^2)]_{2\leftarrow 2}|^2 \times |\vec{k}_2(s=x^2)| x^2 dx, \tag{17}$$

[4] This makes the comparison with Refs. [21,22] more straightforward. One could also take the physical values for these decay constants, but part of the effect can be absorbed into a redefinition of the parameters in Eq. (13). See also Eq. (34) in Ref. [25].

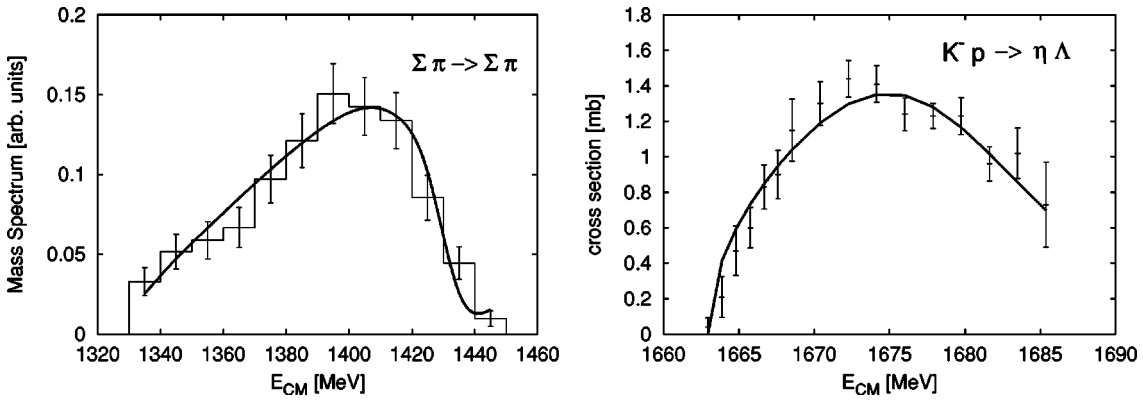

FIG. 2. Solid lines: results of our fit. Experimental data for $\pi\Sigma\to\pi\Sigma$ and $K^-p\to\eta\Lambda$ are from Refs. [37] and [39], respectively.

where C is an arbitrary global normalization factor[5] and i denotes the bin with central c.m. energy $M_{\pi\Sigma}(i)$. Hence, there are only 12 independent data points. Finally, we take the error of the number of counts N_i of the bin i to be $1.61\sqrt{N_i}$ as in Ref. [38].

The $K^-p\to\eta\Lambda$ total cross section of Ref. [39], $1662\leqslant\sqrt{s}\leqslant 1684$ MeV. We use the Crystal Ball Collaboration precise new total cross-section measurements (a total of 17 data points compiled in Table I of Ref. [39]) for the near-threshold reaction $K^-p\to\eta\Lambda$, which is dominated by the $\Lambda(1670)$ resonance. We assume, as in Ref. [39], that the p and higher wave contributions do not contribute to the total cross section.

Finally, we define the χ^2, which is minimized, as

$$\chi^2/N_{\rm tot}=\frac{1}{N}\sum_{\alpha=1}^{N}\frac{1}{n_\alpha}\sum_{j=1}^{n_\alpha}\left(\frac{x_j^{(\alpha)\rm theor}-x_j^{(\alpha)}}{\sigma_j^{(\alpha)}}\right)^2, \qquad (18)$$

where $N=4$ stands for the four sets of data used and discussed above[6] and $x_j^{(\alpha)\rm theor}$ denotes our model result for the data point $x_j^{(\alpha)}$. Finally, n_α takes the values 56, 56, 12, and 17, and $N_{\rm tot}=\Sigma_{\alpha=1}^{N}n_\alpha$ is the total number of data points. With such a definition, acceptable best fits should provide values of $\chi^2/N_{\rm tot}$ around 1.

Although we have considered four coupled channels, three-body channels, for instance the $\pi\pi\Sigma$ one, are not explicitly considered, as was also assumed previously in Refs. [22] and [39].

B. Results of the best χ^2 fit

The model presented up to now has initially 12 free parameters [Eq. (12)], which have to be determined from data. This is a cumbersome task because there are many mathematical minima that are not physically admissible. For instance, in some cases one finds fits to data with spurious poles in the first Riemann sheet which strongly influence the scattering region and hence violate causality. Any fit embodying these singularities is physically inadmissible and should be rejected. This is an important issue, which should always be considered in any analysis. We will further elaborate on this point in Appendix B.

Furthermore, even if one is reasonably convinced that a physically acceptable minimum has been found, there are strong correlations between the fitted parameters, which have to be carefully evaluated and, if possible, understood. Our best results come from a minimum for which the pairs (J_i,Δ_{B_i}) with $i=\bar{K}N$, $\pi\Sigma$, $\eta\Lambda$, $K\Xi$, and $B_i=N$, Σ, Λ, Ξ are totally correlated (correlation factors bigger than 0.99), which leads to an almost singular correlation matrix, reflecting the fact that there exists, in very good approximation, a linear relation between the J_i and Δ_{B_i} parameters.[7] Thus, we have fixed Δ_{B_i} to some specific values in the neighborhood of the minimum, given in Appendix A, and have studied the correlation matrix for the remaining eight parameters. Yet, we find a strong correlation (0.99) between $J_{K\Xi}$ and Δ_K and we proceed as above, i.e., we fix Δ_K and evaluate the correlation matrix and variances for the remaining seven parameters. Thus, at the end of the day we have only seven independent best fit parameters. The best fit parameters, their variances, and the correlation matrix are compiled in Appendix A.

In Figs. 2–4 we compare the results of our best fit with the experimental data. The overall description is remarkably good, at both low energies and the higher end of the considered energy region. In addition, as we will see, the description of the $\Lambda(1405)$ and $\Lambda(1670)$ features is also quite good. Thus, our scheme leads to a much better description of the data than the approach of Ref. [22], as was also the case in the strangeness $S=0$ sector ([25] versus [23]).

For the elastic $\bar{K}N\to\bar{K}N$ scattering length we get

[5]We fix it by setting the area of our theoretical spectrum, $\Sigma_i\Delta\sigma/\Delta[M_{\pi\Sigma}(i)]$, to the total number of experimental counts $\Sigma_i N_i$.

[6]From the first item above and to define the χ^2, we consider two separate sets: $\bar{K}N\to\bar{K}N$ and $\bar{K}N\to\pi\Sigma$.

[7]In Ref. [25] the static limit (infinitely heavy baryons) is discussed, and it is shown [Eq. (D9)] that there exists a linear relation between J_i and Δ_{B_i} if, as is the case here, Δ_{m_i}, $i=\bar{K},\pi,\eta,K$, is small when compared to Δ_{B_i}.

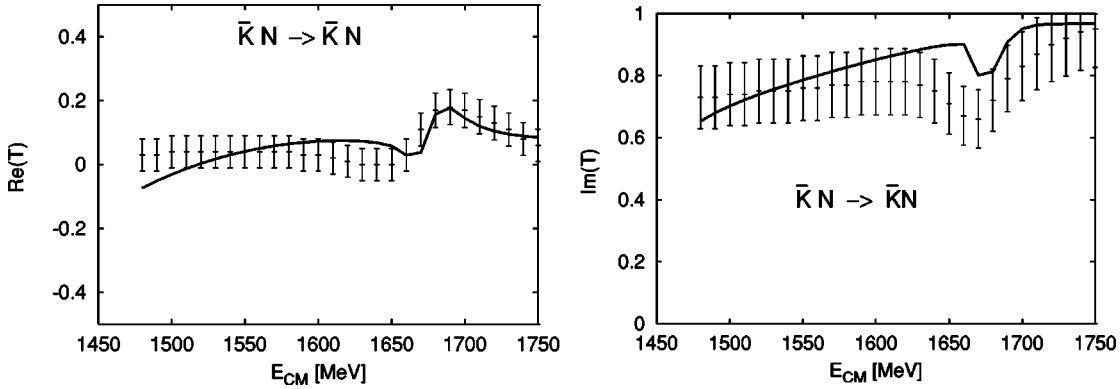

FIG. 3. The real (left panel) and imaginary (right panel) parts of the *s*-wave *T* matrix, with normalization specified in Eq. (16), for the elastic $\bar{K}N \to \bar{K}N$ process in the $I=0$ isospin channel as functions of the c.m. energy. The solid line is the result of our fit, and the experimental data are taken from the analysis of Ref. [35] with the errors stated in the main text.

$$a_{\bar{K}N} \equiv [f_0^{1/2}(s=(m_K+M_N)^2)]_{\bar{K}N \leftarrow \bar{K}N} = (-1.20 \pm 0.09 + i\,1.29 \pm 0.09)\ \text{fm}, \tag{19}$$

where the error is statistical and has been obtained from the covariance matrix given in Appendix A, taking into account the existing statistical correlations, through a Monte Carlo simulation. This value should be compared both to the experimental one $(-1.71+i0.68)$ fm of Ref. [28] and to the LSE approach of Ref. [21] $(-2.24+i1.94)$ fm. Unfortunately, the previous works do not provide error estimates, so one cannot decide on the compatibility of the results.

C. Second Riemann sheet: Poles and resonances

In this section we are interested in describing the masses and widths of the S_{01} resonances in the $S=-1$ channel. Since causality imposes the absence of poles in the $t(s)$ matrix in the physical sheet [40], one should search for complex poles in unphysical ones. Among all of them those *closest* to the physical sheet and hence to the scattering line are the most relevant ones. We define the second Riemann sheet in the relevant fourth quadrant as that which is obtained by continuity across each of the four unitarity cuts (see a detailed discussion in a similar context in Ref. [25]). Physical resonances appear in the second Riemann sheet of all matrix elements of $t(s)$, defined in Eq. (11), in the coupled channel space, differing only on the value of the residue at the pole. The residue determines the coupling of the resonances to the given channel. In Fig. 5 we show the absolute value of the $\eta\Lambda \to \eta\Lambda$ element of the *t* matrix. We choose this channel because all found poles have a sizable coupling to it. Both the fourth quadrant of the second Riemann sheet and the first quadrant of the first (physical) Riemann sheet are shown. The physical scattering takes place in the scattering line in the plot (upper lip of the unitarity cut of the first Riemann sheet). We find three poles in the second Riemann sheet whose positions are $(s=M_R^2-iM_R\Gamma_R)$

$$\text{First pole:} \quad M_R = 1368 \pm 12, \quad \Gamma_R = 250 \pm 23; \tag{20}$$

$$\text{Second pole:} \quad M_R = 1443 \pm 3, \quad \Gamma_R = 50 \pm 7; \tag{21}$$

$$\text{Third pole:} \quad M_R = 1677.5 \pm 0.8, \quad \Gamma_R = 29.2 \pm 1.4, \tag{22}$$

where all units are given in MeV and errors have been transported from those in the best fit parameters [Eq. (A1)], taking into account the existing statistical correlations through a Monte Carlo simulation.

These poles are related to the two S_{01} resonances $\Lambda(1405)$ and $\Lambda(1670)$ which appear up to this range of energy in the

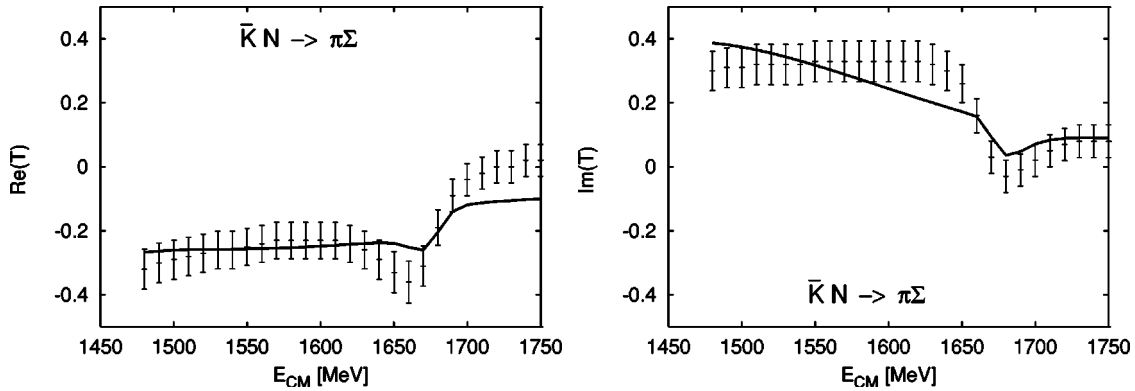

FIG. 4. Same as in Fig. 3 for the inelastic channel $\bar{K}N \to \pi\Sigma$.

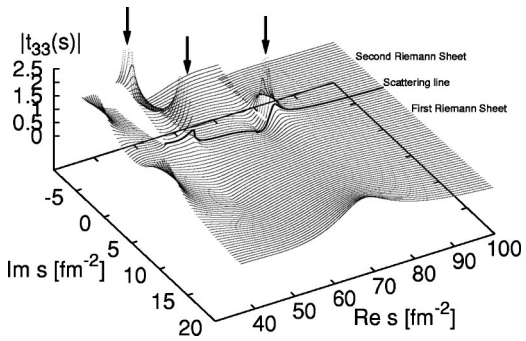

FIG. 5. Modulus of the $\eta\Lambda\to\eta\Lambda$ element of the scattering amplitude $t(s)$ (fm), defined in Eq. (11), analytically extended to the first and fourth quadrants of the s complex plane. The solid line is the scattering line, $s=x+i0^+$, $x\in\mathbb{R}$, from the first threshold $(m_\pi+M_\Sigma)^2$ on. The first (second) Riemann sheet is depicted in the first (fourth) quadrant of the s complex plane. Three poles appear in the second Riemann sheet, which are connected with the $\Lambda(1405)$ and $\Lambda(1670)$ resonances; see the discussion in the main text. Unphysical poles also show up in the physical sheet out of the real axis, but they do not influence the scattering lines as can be seen in the plot.

Particle Data Group (PDG) compilation (Ref. [41]). The third pole above can be clearly identified with $\Lambda(1670)$, which is located at

$$\Lambda(1670):\quad M_R=1670\pm10,\quad \Gamma_R=35^{+15}_{-10},\quad \text{Ref. [41]},$$
$$M_R=1673\pm2,\quad \Gamma_R=23\pm6,\quad \text{Ref. [33]}, \tag{23}$$

where again the units are MeV. The agreement of our predictions and the experimental data is satisfactory and better than in the previous theoretical LSE approach of Ref. [22]. Let us look at the $\Lambda(1405)$ resonance, whose nature is under much discussion [42,43]. Following the PDG, it is placed at (in MeV)

$$\Lambda(1405):\quad M_R=1406.5\pm4.0,\quad \Gamma_R=50\pm2,\quad \text{Ref. [41]}. \tag{24}$$

Our amplitudes have two poles in the region of 1400 MeV, Eqs. (20) and (21). The features of the second one are in agreement with the previous results of Refs. [21,22] and though the width compares well with the experiment, the mass is shifted to higher values. In addition, we should note that the pole quoted in Eq. (20) is very broad and cannot be identified with any of the experimentally established resonances. This pole is also present in the LSE model of Refs. [21,22], as was pointed out in Ref. [44]; although the mass position there is similar ($M_R=1390$ MeV), the width is about a factor of 2 narrower ($\Gamma_R=132$ MeV) than ours. Our understanding is that this broad resonance does not strongly influence the scattering line. However, the $\pi\Sigma$ mass spectrum peaks around 1405 MeV in the experimental data and also in our approach as can be seen in Fig. 2. This is a clear indication of a sizable nonresonant contribution on top of our 1443 MeV pole.

On the other hand, there are unphysical poles in the physical (first) Riemann sheet. These unphysical poles appear because we have truncated the iterated potential to solve the BSE. The two of them closer to the scattering line are located at $(s=M^2+iM\Gamma)$ with $M\approx1166$, $\Gamma\approx\pm200$ MeV and $M\approx1616$, $\Gamma\approx631$ MeV. The tails of both poles can be seen in Fig. 5 and they do not influence the scattering line. In Appendix B, we will show the results from a fit which, at first sight, are in even better agreement with the experimental data (Sec. III A) than those presented up to now. However, this apparent improvement is achieved because the unphysical poles get closer to the real s axis and they affect, in a substantial manner, the scattering amplitudes. Hence, we discard this minimum, and we would like to note that it is important to observe the positions and influence of the unphysical poles when deciding the goodness of a phenomenological description of data.

Finally, we have also analyzed the nature of the resonances in the light of the well known Breit-Wigner (BW) parametrization for coupled channels and real s (see, e.g., Ref. [45] and references therein),

$$t_{ij}^{\rm BW}(s)=-\frac{\delta_{ij}}{2i\rho_i}[e^{2i\delta_i}-1]+\frac{e^{i(\delta_i+\delta_j)}M_R\sqrt{\Gamma_i^{\rm BW}\Gamma_j^{\rm BW}}}{\sqrt{\rho_i\rho_j}[s-M_R^2+iM_R\Gamma_R]}, \tag{25}$$

for which the background is assumed to be diagonal in the coupled channel space, and the relative phase of the resonance to the background and the summed partial decay widths $\Sigma_i\Gamma_i^{\rm BW}=\Gamma_R$ are chosen in such a way that $t_{ij}^{\rm BW}(s)$ exactly satisfies unitarity on the real axis. Here, ρ_i is a kinematic factor defined by the second line of Eq. (31) below. The branching ratio is then defined as $B_i^{\rm BW}=\Gamma_i^{\rm BW}/\Gamma_R$. Subtracting the resonance contribution, Eq. (26), to the total amplitude, we found that for our $\Lambda(1670)$ the background is not a diagonal matrix, since for our t_{ij} matrix we get $2\Sigma_{i<j}|t_{ij}-t_{ij}^{\rm RBW}|^2\approx\Sigma_i|t_{ii}-t_{ii}^{\rm RBW}|^2$ for $s\to M_R^2$, with $t_{ij}^{\rm RBW}$ the second term in Eq. (25). In addition, the BW parametrization suggests a relation between the residue at the pole and the imaginary part of the pole. This relation is true only in the sharp resonance approximation $\Gamma_i^{\rm BW}\ll p_i$ with p_i the c.m. momentum of the decaying state. We have also checked that for our problem this is not the case. Actually, with such a definition we find that $\Sigma_i\Gamma_i^{\rm BW}\approx0.8\Gamma_R$ for $\Lambda(1670)$. This is a simple consequence of the incorrect assumption made in Eq. (25).

D. Branching ratios and couplings of the resonances to different final states

Before going further we would like to make some critical remarks regarding the comparison between ''theory'' and ''experiment.'' Our BSE solution has a very specific energy dependence which, as we saw in Sec. III B, is able to numerically fit experimental data, or rather a partial wave analysis with a given energy dependence. Obviously, the two functional forms are not identical, and it is also fair to say that both incorporate their own biases. There is no reason to expect that they are also numerically alike in the complex

TABLE I. Dimensionless complex couplings $g_i=|g_i|e^{i\phi i}$, defined in Eqs. (26)–(28), for all channels $i=\bar{K}N, \pi\Sigma, \eta\Lambda, K\Xi$, and for the three poles (resonances) quoted in Eqs. (20)–(22). The phases are in radians. Errors are purely statistical and affect the last significant digit.

Resonance	$g_{\bar{K}N}$		$g_{\pi\Sigma}$		$g_{\eta\Lambda}$		$g_{K\Xi}$	
(MeV)	$\|g\|$	ϕ	$\|g\|$	ϕ	$\|g\|$	ϕ	$\|g\|$	ϕ
$M_R=1368$	3.9(1)	−0.59(5)	3.65(8)	−0.73(3)	1.7(2)	3.0(2)	0.29(7)	1.14(13)
$M_R=1443$	3.3(2)	0.72(7)	2.14(16)	1.10(8)	2.2(1)	−2.66(3)	0.23(1)	−0.008(57)
$M_R=1677.5$	0.39(2)	−1.29(4)	0.20(1)	0.77(5)	1.22(3)	2.69(2)	1.64(1)	−0.13(1)

plane.[8] Under these conditions, some parameters, like branching ratios, have a different meaning, since the extrapolation of the resonant contribution to the real s axis is ambiguous. Actually, the ambiguity is enhanced as the resonance becomes wider and as a consequence the definition of a branching ratio becomes model dependent. We explain below our definition of branching ratios and how they are extracted from our amplitude.

Let us consider $s_R=M_R^2-iM_R\Gamma_R$ a pole in the second Riemann sheet of the coupled channel scattering matrix $t(s)$. Then, around the pole, it can be approximated by

$$[t(s)]_{ij}\approx 2M_R\frac{g_{ij}}{s-s_R}, \tag{26}$$

where g_{ij} is the residue matrix. Since t is a complex symmetric matrix (due to time reversal invariance), g is also complex symmetric and its rank is 1 to ensure that $s=s_R$ is a pole of order 1 of the det$[t(s)]$. In this way a nondegenerate resonant state is being described.[9] Under these conditions, g_{ij} turns out to be factorizable:[10]

$$g_{ij}=g_ig_j. \tag{28}$$

The above matrix g_{ij} has only one nonzero eigenvalue $g_1^2+g_2^2+g_3^2+g_4^2$, with g_i the associated eigenvector. The vector g_i determines the coupling of the resonance to the different final states, which are well and unambiguously defined even if the corresponding channels are closed in the decay of the resonance. In Table I we give the complex vectors g_i for the three resonances described in Sec. III C. Unfortunately, the PDG does not provide this kind of information and, instead, branching ratios are given. To extract meaningful branching ratios from our calculation, we have to extrapolate the resonant contribution of the scattering amplitude to the s real axis, which is the only one experimentally accessible. In addition, the picture of a resonance as a quantum mechanical decaying state requires a probabilistic description. Thus, we isolate the resonant contribution to the S matrix[11] for $s=M_R^2$

$$S_{ij}^{\text{resonant}}(s=M_R^2)=-2i2M_R\sqrt{\rho_i^R}\frac{g_ig_j}{M_R^2-s_R}\sqrt{\rho_j^R},$$

$$\rho_i(s)=\Theta(s-s_{\text{th}}^i)\frac{|\vec{k}_i(s)|}{8\pi\sqrt{s}}\left(\sqrt{M_i^2+\vec{k}_i^2}+M_i\right),$$

$$\rho_i^R=\rho_i(s=M_R^2), \tag{31}$$

with s_{th}^i the threshold of the baryon-meson channel i. This definition embodies a sensible kinematic suppression compatible with Cutkosky's rules and the s-wave nature of the resonance. Defining

$$b_i=g_i\sqrt{2\rho_i^R/\Gamma_R}, \tag{32}$$

we find

$$S_{ij}^{\text{resonant}}(s=M_R^2)=-2iM_R\Gamma_R\frac{b_ib_j}{M_R^2-s_R}, \tag{33}$$

and, taking into account that the matrix $b_{ij}=b_ib_j$ has rank 1

[8] A good example of this fact is provided by our best fit results of Sec. III B and the physically inadmissible results of Appendix B; they look very much the same on the scattering line although the analytic structure is rather different.

[9] This can be seen as follows. Using matrix notation, the BSE reads $t(s)=V+VG_0(s)t(s)$ and it is solved by $t(s)=V(1-G_0(s)V)^{-1}$, with the obvious identifications for V and G_0. A pole at $s=s_R$ in det$[t(s)]$ is produced by a zero of det$[1-G_0(s)V]$. This last condition ensures that the homogeneous (quasi)bound state Bethe-Salpeter equation

$$[-G_0(s)^{-1}+V]\Psi=0 \tag{27}$$

has a nontrivial solution for $s=s_R$. Indeed, all solutions Ψ of the above equation are linear combinations of the null eigenvectors of the $(1-G_0(s_R)V)$ matrix and describe the dynamics of the existing states (resonances) at $s=s_R$. For a nondegenerate resonance (which we have checked is indeed the case), the zero eigenspace should have dimension 1, whence for the case of four coupled channels, the rank of the matrix $(1-G_0(s_R)V)$ is 3 and therefore det$[1-G_0(s)V]$ should have a single zero at $s=s_R$.

[10] The symmetric complex matrix g can be diagonalized by a complex orthogonal transformation U as $g=U^TdU$, where only one element of the diagonal matrix d is different from zero. If we take this element to be d_{11}, we have $g_{ij}=(U^T)_{i1}d_{11}U_{1j}=d_{11}U_{1i}U_{1j}$.

[11] The S matrix is related to the t matrix, in our convention, by

$$S_{ij}(s)=\delta_{ij}-2i\sqrt{\rho_i(s)}t_{ij}(s)\sqrt{\rho_j(s)}, \tag{29}$$

and probability conservation $(S^\dagger S=SS^\dagger=1)$ holds since t satisfies coupled channel unitarity:

$$t_{ij}^*(s)-t_{ij}(s)=2i\sum_k t_{ik}^*(s)\rho_k(s)t_{kj}(s). \tag{30}$$

and that b_i (or any vector proportional to it) is the only eigenvector of S^{resonant} with a nonzero eigenvalue, the resonant state at $s=M_R^2$ will be given by

$$|R\rangle \propto \sum_i b_i |i\rangle, \tag{34}$$

where $|i\rangle$ stands for the meson-baryon states used to build the coupled channel space. Finally, the branching ratio B_i will be given by the probability of finding $|R\rangle$ in the state $|i\rangle$:

$$B_i = \frac{|b_i|^2}{\Sigma_j |b_j|^2} \tag{35}$$

which by definition satisfies $\Sigma_i B_i = 1$. The partial decay width may then be defined as $\Gamma_i = B_i \Gamma_R$, and obviously $\Sigma_i \Gamma_i = \Gamma_R$. For $\Lambda(1670)$ we obtain the following branching ratios with the above prescription:

$$B_{\bar{K}N} = 0.24 \pm 0.01, \quad B_{\pi\Sigma} = 0.08 \pm 0.01, \quad B_{\eta\Lambda} = 0.68 \pm 0.01. \tag{36}$$

The last two values are not in agreement with the values quoted by the PDG [41] ($B_{\bar{K}N} = 0.25 \pm 0.05$, $B_{\pi\Sigma} = 0.40 \pm 0.15$, $B_{\eta\Lambda} = 0.17 \pm 0.07$) and in Ref. [33] ($B_{\bar{K}N} = 0.37 \pm 0.07$, $B_{\pi\Sigma} = 0.39 \pm 0.08$, $B_{\eta\Lambda} = 0.16 \pm 0.06$, $B_{\pi\Sigma(1385)} = 0.08 \pm 0.06$).

To finish this subsection, we would like to point out that in the present context the concept of the branching ratio is subtle and it might be ambiguous, from both the theoretical and experimental sides. From the experimental point of view the difficulty arises from the impossibility of preparing a pure short-lived resonant state strongly coupled to a continuum, and therefore the impossibility of disentangling events coming from the formation of the resonance from those produced through nonresonant processes. From the theoretical point of view the ambiguity comes when defining $S^{\text{resonant}}(s=M_R^2)$ in Eq. (31). For instance, at the pole $s=s_R$ one could have

$$[t(s)]_{ij} \approx 2M_R \frac{\beta_i(s)}{\beta_i(s_R)} \frac{g_{ij}}{s-s_R} \frac{\beta_j(s)}{\beta_j(s_R)}, \tag{37}$$

instead of the expression assumed in Eq. (26), $\beta_i(s)$ being an arbitrary complex function analytical around s_R. In these circumstances the matrix S_{ij}^{resonant} $(s=M_R^2)$ would be different from that given in Eq. (31) by a factor $[\beta_i(M_R^2)/\beta_i(s_R)][\beta_j(M_R^2)/\beta_j(s_R)]$ and one would get a new vector $\tilde{b}_i$, which in terms of the vector b_i, defined in Eq. (32), reads

$$\tilde{b}_i = \frac{\beta_i(M_R^2)}{\beta_i(s_R)} b_i, \tag{38}$$

leading, in principle, to different branching ratios. The trouble comes from the extrapolation from s_R to the real axis, which is not unique.

The usual assumption is that the $\beta_i(s)$ functions are smooth and they do not change much from $s=s_R$ to $s=M_R^2$, and, more important, that the change does not depend significantly on the channel i. However, this is not always true; for example, if one were dealing with a p-wave resonance the function $\beta_i(s)$ would at least include the c.m. meson-baryon momentum. If there is a channel that becomes open close to and above $s=M_R^2$, then the c.m. momentum will lead to a suppression of the branching ratio to this channel.

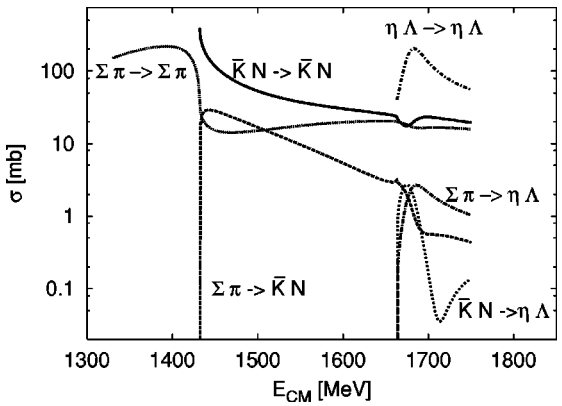

FIG. 6. $I=0$ meson-baryon s-wave cross sections for different channels.

E. Predictions for other processes

In Fig. 6 we show some of our predictions for s-wave $I=0$ cross sections for some elastic and inelastic channels. For most of them there are no data. The effect of the $\Lambda(1405)$ resonance is clearly visible in the $\Sigma\pi \to \Sigma\pi$, $\Sigma\pi \to \bar{K}N$, and $\bar{K}N \to \bar{K}N$ cross sections. On the other hand, the elastic $\eta\Lambda$ cross section takes a very large value at threshold, which corresponds to a typical low energy resonance behavior triggered by the $\Lambda(1670)$ resonance. This is in contrast to any expectation based on the Born approximation, since the corresponding potential in this channel vanishes [Eq. (9)]. Our estimates for the $\pi\Sigma$ and $\eta\Lambda$ scattering lengths [defined for the elastic channels as in Eq. (19)] are

$$a_{\pi\Sigma} = 1.10 \pm 0.06 \text{ fm},$$
$$a_{\eta\Lambda} = (0.50 \pm 0.05) + i(0.27 \pm 0.01) \text{ fm}, \tag{39}$$

respectively.

F. Heavy baryon expansion at threshold

As we have already mentioned, the only calculation within HBChPT in the $S=-1$ sector is that of Ref. [27], where the s-wave scattering lengths in both isospin channels $I=0$ and 1 are computed. It is found that HBChPT to one loop fails completely in the $I=0$ channel due to the strong influence of the subthreshold $\Lambda(1450)$ resonance. We think that it is of interest to analyze this problem within the context of our unitarization approach.

As was discussed previously by two of us [25], the condition for the coupled channel amplitude to have a well defined static limit $M \to \infty$ is that the combination

$$C_{\hat{m}\hat{M}} = \frac{1}{\hat{m}} \left[\hat{M} J_{\hat{m}\hat{M}} + \frac{1}{4\hat{M}} (\Delta_{\hat{m}} - \Delta_{\hat{M}}) \right] \tag{40}$$

goes to some definite finite value. The parameters $J_{\hat{m}\hat{M}}$ and $\Delta_{\hat{m}}$ and $\Delta_{\hat{M}}$ are listed in Eq. (13) and their best fit result is presented in Eq. (A1) of Appendix A. Using Eq. (A1) one can estimate the combinations in units of the relevant meson mass:

$$
\begin{aligned}
M_\Sigma J_{\pi\Sigma}+\frac{\Delta_\pi-\Delta_\Sigma}{4M_\Sigma}&=+0.24m_\pi,\\
M_N J_{\bar{K}N}+\frac{\Delta_{\bar{K}}-\Delta_N}{4M_N}&=-0.09m_{\bar{K}},\\
M_\Lambda J_{\eta\Lambda}+\frac{\Delta_\eta-\Delta_\Lambda}{4M_\Lambda}&=+0.08m_\eta,\\
M_\Xi J_{K\Xi}+\frac{\Delta_K-\Delta_\Xi}{4M_\Xi}&=-0.64m_K,
\end{aligned}
\tag{41}
$$

showing that they are not unnaturally large. Following the discussion of Ref. [25], the heavy baryon expansion is done in the standard way, and taking the leading heavy baryon approximation of the parameters,

$$
\begin{aligned}
J_{\hat{m}\hat{M}}&=J^0_{\hat{m}\hat{M}}\left\{1+\mathcal{O}\left(\frac{1}{M}\right)\right\},\\
\Delta_{\hat{m}}&=\Delta^0_{\hat{m}}\left\{1+\mathcal{O}\left(\frac{1}{M}\right)\right\},\\
\Delta_{\hat{M}}&=\Delta^0_{\hat{M}}\left\{1+\mathcal{O}\left(\frac{1}{M}\right)\right\},
\end{aligned}
\tag{42}
$$

we get for the $\bar{K}N$ s-wave scattering length in the $I=0$ channel the following expression:

$$
\begin{aligned}
a_{\bar{K}N}=&\frac{3m_{\bar{K}}}{8\pi f_K^2}\left[1-\frac{m_{\bar{K}}}{M_N}+\frac{m_{\bar{K}}^2}{M_N^2}\right]+\frac{9}{16\pi f_K^4}\left(\frac{3}{4}\Delta^0_{\bar{K}}m_{\bar{K}}-2C^0_{KN}m_{\bar{K}}^3\right)+\frac{3}{32\pi f_K^2 f_\pi^2}\left\{\frac{3}{4}\Delta^0_\pi m_{\bar{K}}-2C^0_{\pi\Sigma}m_{\bar{K}}^2 m_\pi\right.\\
&-\frac{1}{4\pi^2}m_{\bar{K}}^2\sqrt{m_{\bar{K}}^2-m_\pi^2}\left[\operatorname{arccosh}\left(\frac{m_\pi}{m_{\bar{K}}}\right)-i\pi\right]-\frac{1}{4\pi^2}m_{\bar{K}}^2(m_\pi-m_{\bar{K}})\ln\frac{M_\Sigma}{m_\pi}\left.\right\}+\frac{9}{32\pi f_K^2 f_\eta^2}\left\{\frac{3}{4}\Delta^0_\eta m_{\bar{K}}-2C^0_{\eta\Lambda}m_{\bar{K}}^2 m_\eta\right.\\
&-\frac{1}{4\pi^2}m_{\bar{K}}^2\sqrt{m_\eta^2-m_{\bar{K}}^2}\arccos\left(-\frac{m_{\bar{K}}}{m_\eta}\right)-\frac{1}{4\pi^2}m_{\bar{K}}^2(m_\eta-m_{\bar{K}})\ln\frac{M_\Lambda}{m_\eta}\left.\right\}+\mathcal{O}\left(\frac{1}{f^2M^3},\frac{1}{Mf^4},\frac{1}{f^6}\right).
\end{aligned}
\tag{43}
$$

This expression can be mapped into the HBChPT result of Ref. [27], since the transcendental function dependence is exactly the same. This should be so because the authors of [27] build the perturbative unitarity correction in HBChPT. Thus, one could identify a linear combination of the leading order approximation of our constants, with another linear combination of HBChPT constants. On the other hand, if we assume the values of the best fit parameters, Eq. (A1), for $J^0_{\hat{m}\hat{M}}$, $\Delta^0_{\hat{m}}$, and $\Delta^0_{\hat{M}}$ we obtain the following numerical estimate:

$$
\begin{aligned}
a_{\bar{K}N}=&\underbrace{1.02}_{1/f^2}-\underbrace{0.53}_{1/f^2M}+\underbrace{0.28}_{1/f^2M^2}+\underbrace{\overbrace{1.00+i0.41}^{\pi\Sigma}-\overbrace{1.25}^{\bar{K}N}+\overbrace{3.17}^{\eta\Lambda}}_{1/f^4}+\cdots\\
=&3.69+i0.41\ \text{fm}+\cdots,
\end{aligned}
\tag{44}
$$

where the contributions are separated according to the order in the chiral expansion and also to the corresponding intermediate state. As we see, large cancellations at higher orders must take place to obtain, after summing the whole series, our result in Eq. (19). Note also that the real part is about twice as large and with opposite sign as compared to the experimental result [28]. A similar situation occurs in HBChPT [27]; the real part of the scattering amplitude has the opposite sign although a similar magnitude to the experimental number. Likewise, large cancellations have also been noted, indicating a bad convergence rate in HBChPT. The fact that our calculation Eq. (44) gives a larger magnitude for $\mathrm{Re}\,a_{\bar{K}N}$ than in HBChPT reflects, in addition, a bad convergence in the expansion (43). This situation has also been described in the coupled channel case $S=0$ sector [25] and seems a common feature of unitarization methods [12–14].

IV. CONCLUSIONS

In this paper we extended the Bethe-Salpeter formalism developed in Ref. [25] to study s-wave and $I=0$ meson-baryon scattering up to 1.75 GeV in the strangeness $S=-1$ sector. We work on a four-dimensional two-body channel space and the kernel of the BSE takes into account CS constraints as deduced from the corresponding effective Lagrangian. The t matrix obtained manifestly complies with coupled channel unitarity and the undetermined low energy constants of the model have been fitted to data. The available direct experimental information is limited to the $\pi\Sigma\to\pi\Sigma$ mass spectrum, and the $K^-p\to\Lambda\eta$ total cross section, for which errors are provided, and to the $\bar{K}N\to\bar{K}N$ and $\bar{K}N\to\pi\Sigma$ scattering amplitudes of a partial wave analysis, for which errors are guessed. Taking this into account, the agreement with experiment is satisfactory. In addition, some predictions for other cross sections, not yet measured, have also been given. A careful and detailed statistical study has been carried out, showing that only seven parameters (LEC's) out of the starting 12 are really independent. Thus, although our model has more free parameters than those required in Ref. [22], the description of data achieved in our approach is su-

perior to that of Ref. [22]. A similar situation was already found in the strangeness $S=0$ sector also [25]. According to previous experience, the reduction of parameters is partly due to the constraint of a well defined heavy baryon limit [25]. Likewise, crossing symmetry is expected to shed more light on the number of independent LEC's. As we have argued, matching to HBChPT calculations in the $S=-1$ and $I=0$ sector would be the ideal way to map our LEC's into those stemming from an effective chiral Lagrangian, but it is already known that the chiral expansion fails [27] to reproduce the $\bar{K}N$ scattering length, due to the influence of the nearby subthreshold $\Lambda(1405)$ resonance. Possibly this could be overcome by properly accounting for the singularity structure as suggested in [15]. We believe these points deserve a deeper investigation.

We have undertaken a careful discussion on the analytical structure of the scattering matrix amplitude in the complex s plane, which becomes mandatory in order to extract the features of the S_{01} resonances. We have searched for poles in the second Riemann sheet and compared masses; widths, and branching ratios to data. The agreement is also quite satisfactory. In the resonance region our unitary amplitude cannot be analyzed as a Breit-Wigner resonance due to a sizably nondiagonal background in coupled channel space. This, in particular, prevents a simple interpretation of branching ratios. Although residues at the resonance poles are well and unambiguously defined, the definition of branching ratios requires special considerations and provisos, due to an ambiguous extrapolation of the resonance contribution of the S matrix from the pole to the scattering line. We have also illustrated that looking for a good description of experimentally accessible data is not sufficient and that, in some cases, it can be achieved at the expense of generating nonphysically acceptable poles in the first Riemann sheet, which influence on the scattering region is non-negligible. Thus, any fit to data should be supplemented by this additional requirement of not producing spurious singularities numerically relevant for the description of scattering processes.

ACKNOWLEDGMENTS

We warmly thank E. Oset and A. Ramos for useful discussions. This research was supported by DGES under Contracts No. BFM2000-1326 and No. PB98-1367 and by the Junta de Andalucia.

APPENDIX A: BEST FIT RESULTS

The best fit ($\chi^2/N_{\rm tot}=0.93$) parameters are

$$\begin{aligned} J_{\bar{K}N} &= -0.0186 \pm 0.0010, \\ J_{\pi\Sigma} &= 0.00796 \pm 0.00061, \\ J_{\eta\Lambda} &= 0.01264 \pm 0.00021, \\ J_{K\Xi} &= -0.11936 \pm 0.00018, \\ \bar{\Delta}_N \equiv \Delta_N/(m_{\bar{K}}+M_N)^2 &= 0.01355 \pm 0.00029, \\ \bar{\Delta}_\Sigma \equiv \Delta_\Sigma/(m_\pi+M_\Sigma)^2 &= -0.00325 \pm 0.00036, \\ \bar{\Delta}_\Lambda \equiv \Delta_\Lambda/(m_\eta+M_\Lambda)^2 &= -0.00262 \pm 0.00011, \end{aligned} \tag{A1}$$

with fixed parameters

$$\begin{aligned} \Delta_\Xi/(m_K+M_\Xi)^2 &= -0.0035, \\ \Delta_{\bar{K}}/(m_{\bar{K}}+M_N)^2 &= -0.034, \\ \Delta_\pi/(m_\pi+M_\Sigma)^2 &= 0.060, \\ \Delta_\eta/(m_\eta+M_\Lambda)^2 &= 0.049, \\ \Delta_K/(m_K+M_\Xi)^2 &= -0.26, \end{aligned} \tag{A2}$$

as explained in the main text. We assume that the parameters of Eq. (A1) are Gaussian correlated; this is justified because they come from a χ^2 fit. To make any further statistical analysis of quantities derived from the parameters above, the corresponding covariance (v) and correlation (c) matrices are needed. These matrices are defined as usual:

$$\begin{aligned} v_{ij} &= \left[\left(\frac{1}{2}\frac{\partial\chi^2}{\partial b_k \partial b_l}\right)^{-1}\right]_{ij}, \\ c_{ij} &= v_{ij}/\sqrt{v_{ii}v_{jj}}, \end{aligned} \tag{A3}$$

b_i being any of the seven parameters J and Δ of Eq. (A1). The errors δb_i quoted in Eq. (A1) are obtained from the diagonal elements of the covariance matrix ($\delta b_i=\sqrt{v_{ii}}$). Finally, our estimate for the correlation matrix reads

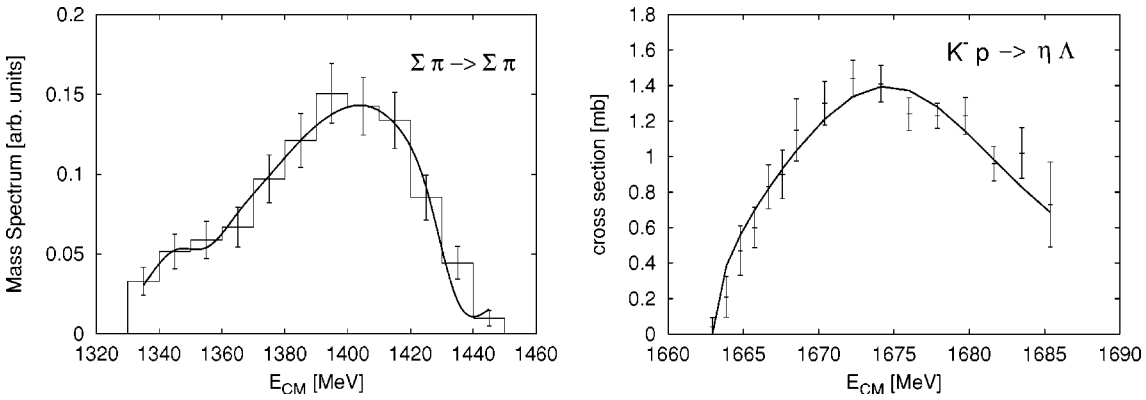

FIG. 7. Same as Fig. 2 for the nonphysically acceptable fit described in Appendix B.

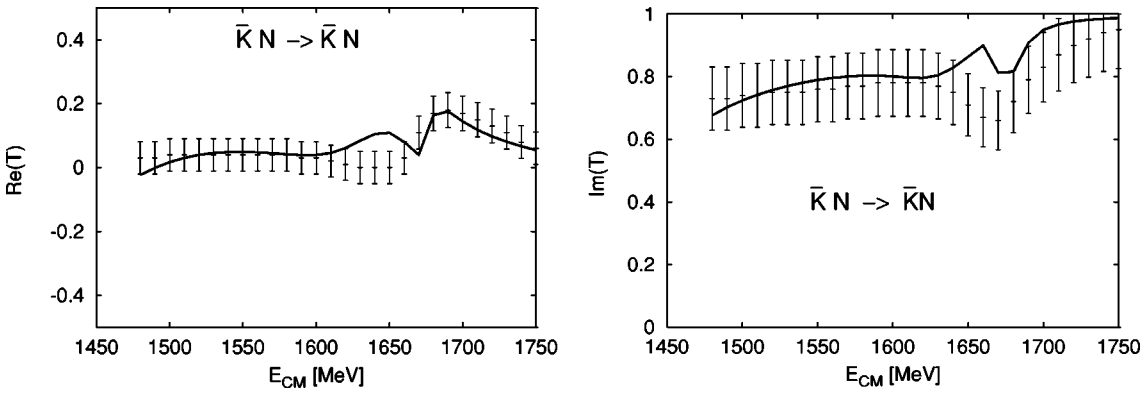

FIG. 8. Same as Fig. 3 for the nonphysically acceptable fit described in Appendix B.

$$
\begin{pmatrix}
 & J_{\bar{K}N} & J_{\pi\Sigma} & J_{\eta\Lambda} & J_{K\Xi} & \bar{\Delta}_N & \bar{\Delta}_\Sigma & \bar{\Delta}_\Lambda \\
J_{\bar{K}N} & 1.000 & & & & & & \\
J_{\pi\Sigma} & -0.236 & 1.000 & & & & & \\
J_{\eta\Lambda} & -0.909 & 0.442 & 1.000 & & & & \\
J_{K\Xi} & 0.569 & -0.479 & -0.530 & 1.000 & & & \\
\bar{\Delta}_N & -0.830 & 0.228 & 0.702 & -0.829 & 1.000 & & \\
\bar{\Delta}_\Sigma & 0.294 & 0.608 & -0.030 & 0.224 & -0.494 & 1.000 & \\
\bar{\Delta}_\Lambda & -0.158 & -0.501 & 0.087 & 0.613 & -0.336 & -0.051 & 1.000
\end{pmatrix}. \tag{A4}
$$

Even though the correlations in the above matrix have at most a modulus of about 0.9, the matrix has an eigenvalue quite close to zero (0.0025), which is a clear indication that one of the parameters might still be redundant.

APPENDIX B: NONPHYSICALLY ACCEPTABLE FITS TO DATA

In Figs. 7–9 we present the results of a fit to the data, that we will show is not physically acceptable. The overall description of the data is remarkably good. This fit gives $\chi^2/N_{\rm tot}=0.69$, to compare with the value of 0.93 of the best fit presented in the main text. However, on looking at the $t(s)$ matrix in the s complex plane (Fig. 10), one realizes that there exist a proliferation of poles, some of them unphysical and others with no experimental counterparts. In the first Riemann sheet we find at least two poles. The first one is located at $s=M^2-iM\Gamma$ with $M=1606$ MeV and $\Gamma=153$ MeV. This pole is close to the s real axis and produces visible effects on the scattering line not only for the $t_{\eta\Lambda\to\eta\Lambda}$ entry shown in the figure, but also for all $i\to j$ channels. Indeed, as we showed in Sec. III C, our preferred fit also has a similar unphysical pole but significantly farther ($\Gamma=631$ MeV) from the real axis, and therefore with a tiny

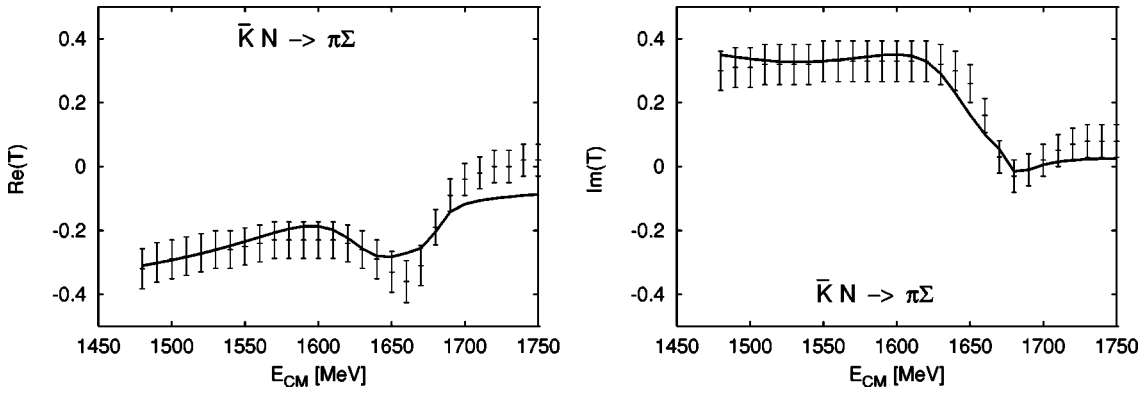

FIG. 9. Same as Fig. 8 for the inelastic channel $\bar{K}N\to\pi\Sigma$.

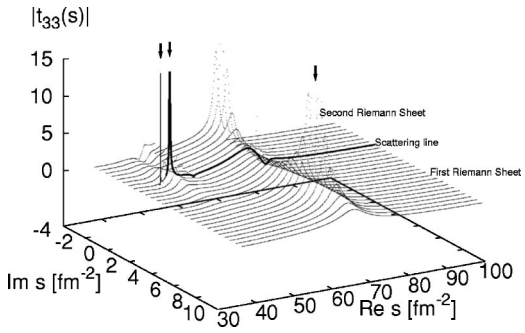

FIG. 10. Same as Fig. 5 for the nonphysically acceptable fit to the data described in Appendix B.

influence on the physical scattering. Since causality imposes the absence of poles in the physical sheet [40], the existence of such a pole affecting the scattering line invalidates the description (Figs. 7–9) presented in this appendix, despite its quality. Also, in the first sheet, there exists a pole on the real axis ($\sqrt{s}=1307$ MeV) and below the first threshold, which would correspond to a bound state, stable under strong interactions. Such a state has the same quantum numbers as $\Lambda(1115)$ and it should show up in all reactions where the latter is produced.

On the other hand, in the second sheet there now exist four poles. Three of them are similar to those presented in Sec. III C, although the one placed around 1370 MeV [Eq. (20)] is now almost a factor of 2 narrower (it is located at $M_R=1392$ MeV and $\Gamma_R=120$ MeV). In addition there exists a new resonance $M_R=1343$ MeV and $\Gamma_R=0.18$ MeV which is responsible for the high peak at the beginning of the scattering line in Fig. 10 and for the existing bump between 1330 and 1360 MeV in the $\pi\tilde{\Sigma}$ mass spectrum of Fig. 7. As far as we know, there are no other independent indications of the existence of this extremely narrow resonance.

We have presented the results of this nonphysically acceptable fit to stress that, in order to be sure of having a good approach to the t matrix of a given physical system, one should *not only* look at the t matrix and related observables (cross sections, etc.) at the physical scattering line (real s values), but *also* study its behavior on the s complex plane, both in the second Riemann sheet to find the resonances and in the first Riemann sheet to be sure of avoiding pathological behaviors such as the one illustrated in Fig. 10.

[1] For a review, see, e.g., M. Arima, K. Masutani, and T. Sato, Prog. Theor. Phys. Suppl. **137**, 169 (2000).
[2] A. Pich, Rep. Prog. Phys. **58**, 563 (1995).
[3] E. Jenkins and A. V. Manohar, Phys. Lett. B **255**, 558 (1991).
[4] V. Bernard, N. Kaiser, J. Kambor, and Ulf G. Meissner, Nucl. Phys. **B388**, 315 (1992).
[5] M. Mojzis, Eur. Phys. J. C **2**, 181 (1998).
[6] N. Fettes, Ulf G. Meissner, and S. Steininger, Nucl. Phys. **A640**, 199 (1988).
[7] N. Fettes and Ulf G. Meissner, Nucl. Phys. **A676**, 311 (2000).
[8] T. Becher and H. Leutwyler, Eur. Phys. J. C **9**, 643 (1999).
[9] T. Becher and H. Leutwyler, J. High Energy Phys. **06**, 017 (2001).
[10] N. Fettes and U. G. Meissner, Nucl. Phys. **A679**, 629 (2001).
[11] K. Torikoshi and P. J. Ellis, Phys. Rev. C **67**, 015208 (2003).
[12] A. Gómez Nicola and J. R. Peláez, Phys. Rev. D **62**, 017502 (2000).
[13] J. Nieves and E. Ruiz Arriola, hep-ph/0001013; Gómez Nicola, J. Nieves, J. R. Peláez, and E. Ruiz Arriola, Phys. Lett. B **486**, 77 (2000).
[14] J. Nieves and E. Ruiz Arriola, Phys. Rev. D **63**, 076001 (2001).
[15] U. G. Meissner and J. A. Oller, Nucl. Phys. **A673**, 311 (2000).
[16] J. A. Oller and Ulf. G. Meissner, Phys. Lett. B **500**, 263 (2001).
[17] N. Kaiser, P. B. Siegel, and W. Weise, Nucl. Phys. **A594**, 325 (1995).
[18] N. Kaiser, P. B. Siegel, and W. Weise, Phys. Lett. B **362**, 23 (1995).
[19] N. Kaiser, T. Waas, and W. Weise, Nucl. Phys. **A612**, 297 (1997).
[20] J. Caro Ramon, N. Kaiser, S. Wetzel, and W. Weise, Nucl. Phys. **A672**, 249 (2000).
[21] E. Oset and A. Ramos, Nucl. Phys. **A635**, 99 (1998).
[22] E. Oset, A. Ramos, and C. Bennhold, Phys. Lett. B **527**, 99 (2002); **530**, 260(E) (2002).
[23] J. C. Nacher, A. Parreño, E. Oset, A. Ramos, A. Hosaka, and M. Oka, Nucl. Phys. **A678**, 187 (2000).
[24] T. Inoue, E. Oset, and M. J. Vicente-Vacas, Phys. Rev. C **65**, 035204 (2002).
[25] J. Nieves and E. Ruiz Arriola, Phys. Rev. D **64**, 116008 (2001).
[26] M. F. M. Lutz and E. E. Kolomeitsev, Nucl. Phys. **A700**, 193 (2002).
[27] N. Kaiser, Phys. Rev. C **64**, 045204 (2001).
[28] A. D. Martin, Nucl. Phys. **B179**, 33 (1981).
[29] J. Nieves and E. Ruiz Arriola, Phys. Lett. B **455**, 30 (1999); Nucl. Phys. **A679**, 57 (2000).
[30] C. Garcia-Recio, J. Nieves, E. Ruiz Arriola, and M. Vicente Vacas, in Proceedings of Conference on Quarks and Nuclear Physics (QNP 2002), Julich, Germany, 2002, nucl-th/0209053.
[31] C. Garcia-Recio, J. Nieves, E. Ruiz Arriola, and M. Vicente Vacas, in Proceedings of PANIC02, Osaka, Japan, 2002 (to appear).
[32] C. Garcia-Recio, J. Nieves, E. Ruiz Arriola, and M. Vicente Vacas, in Proceedings of 2nd International Workshop on Hadron Physics: Effective Theories of Low-Energy QCD, Coimbra, Portugal, 2002, nucl-th/0211098.
[33] D. M. Manley *et al.*, Phys. Rev. Lett. **88**, 012002 (2002).
[34] T. Hyodo, S. I. Nam, D. Jido, and A. Hosaka, nucl-th/0212026.
[35] G. P. Gopal *et al.*, Nucl. Phys. **B119**, 362 (1977).
[36] M. Th. Keil, G. Penner, and U. Mosel, Phys. Rev. C **63**, 045202 (2001).
[37] R. J. Hemingway, Nucl. Phys. **B253**, 742 (1984).
[38] R. H. Dalitz and A. Deloff, J. Phys. G **17**, 289 (1991).
[39] A. Starostin *et al.*, Phys. Rev. C **64**, 055205 (2001).

[40] S. Mandelstam, Phys. Rev. **112**, 1344 (1958).
[41] K. Hagiwara *et al.*, Phys. Rev. D **66**, 010001 (2002).
[42] R. H. Dalitz, Eur. Phys. J. C **3**, 676 (1998).
[43] M. Kimura, T. Miyakawa, A. Suzuki, M. Takayama, K. Tanaka, and A. Hosaka, Phys. Rev. C **62**, 015206 (2000).
[44] D. Jido, A. Hosaka, J. C. Nacher, E. Oset, and A. Ramos, Phys. Rev. C **66**, 025203 (2002).
[45] A. M. Badalyan, L. P. Kok, M. L. Polykarpov, and Yu. A. Simonov, Phys. Rep. **82**, 31 (1982).